Supplementary Information

Thermal Activation of Methane by Vanadium Boride Cluster Cations VB_n^+ (n = 3–6)

Qiang Chen,[ab] Yan-Xiao Zhao,*[ab] Li-Xue Jiang,[abc] Hai-Fang Li,[ab] Jiao-Jiao Chen,[abc] Ting Zhang,[abc] Qing-Yu Liu,[ab] and Sheng-Gui He*[abc]

[a] *State Key Laboratory for Structural Chemistry of Unstable and Stable Species, Institute of Chemistry, Chinese Academy of Sciences, Beijing 100190, China*

[b] *Beijing National Laboratory for Molecular Sciences, CAS Research/Education Center of Excellence in Molecular Sciences, Beijing 100190, China*

[c] *University of Chinese Academy of Sciences, Beijing 100049, China*

E-mail: chemzyx@iccas.ac.cn, shengguihe@iccas.ac.cn.

Experimental and Theoretical methods

The VB_n^+ clusters were generated by laser ablation of a rotating and translating V/B mixed disk (V/B molar ratio of 1:10) in the presence of pure He carrier gas (99.999%) with the backing pressure of 6.5 atm. The clusters of interest [VB_n^+ (n = 3-6)] were mass-selected by a quadrupole mass filter and entered into a linear ion trap (LIT) reactor, where they were thermalized by collisions with a pulse of He gas and then interacted with a pulse of Ar, CH_4, or CD_4 for around 1.9 ms. The ions ejected from the LIT were detected by a reflectron time-of-flight mass spectrometer. The details of running the time-of-flight mass spectrometer,[S1] quadrupole mass filter,[S2] and the LIT[S3] can be found in our previous works.

Density functional theory (DFT) calculations using Gaussian 09 package[S4] were carried out to investigate the structures of VB_3^+ and the reaction mechanism of VB_3^+ with CH_4. The reaction mechanism of B_3 + CH_4 was also studied for comparison. In order to find an appropriate functional, the bond dissociation energies (BDEs) of V–C, V–H, B–C, B–H, C–H and H–H were computed by various functionals with TZVP basis sets[S5] and compared with available experimental data[S6] (Table S1). It turns out that M06L functional[S7] was the overall best functional, thus the M06L results were given throughout this work. A Fortran code[S8] based on the genetic algorithm was used to search the global minimum structures of VB_3^+, $VB_3CH_2^+$ and B_3CH_3 with different spin multiplicities. The reaction mechanism calculations involved geometry optimization of reaction intermediates and transition states (TSs). The initial guess structures of the TS species were obtained through relaxed potential energy surface scans using a single or multiple internal coordinates.[S9] The TSs were optimized with Berny algorithm.[S10] Vibrational frequency calculations were performed to check that reaction intermediates and TSs have zero and one imaginary frequencies, respectively. The intrinsic reaction coordinate (IRC)[S11] calculations were carried out to make sure that each TS connects two appropriate minima. The zero-point vibration corrected energies (ΔH_0) were reported in this work. The NBO 3.1 program[S12] was used to calculate the natural atomic charges.

Table S1. Experimental and DFT calculated bond dissociation energies (BDEs) of V–C, V–H, B–C, B–H, C–H, and H–H. The values are given in unit of eV.

	BDEs / eV							Average deviation / eV
	V–B	V–C	V–H	B–C	B–H	C–H	H–H	All species
Expt.[S6]	**–**	**4.43**	**2.16**	**4.64**	**3.52**	**3.51**	**4.52**	
M06L	**2.31**	**4.41**	**2.53**	**4.81**	**3.39**	**3.36**	**4.22**	**-0.01 ± 0.24**
B3LYP	2.12	3.26	2.79	4.37	3.48	3.49	4.50	-0.15 ± 0.58
BP86	2.79	4.82	2.84	4.82	3.51	3.60	4.56	0.23 ± 0.26
B1LYP	1.98	3.44	2.77	4.23	3.42	3.42	4.44	-0.18 ± 0.52
BPW91	2.55	4.53	2.57	4.80	3.35	3.42	4.31	0.03 ± 0.24
X3LYP	2.11	3.22	2.80	4.37	3.47	3.48	4.47	-0.16 ± 0.60
B3P86	2.22	3.91	2.74	4.64	3.54	3.58	4.58	0.04 ± 0.35
B3PW91	2.08	3.62	2.55	4.56	3.39	3.41	4.37	-0.15 ± 0.38
B1B95	1.90	3.51	2.53	4.47	3.40	3.35	4.38	-0.19 ± 0.41
PBE1PBE	2.08	3.50	2.51	4.59	3.34	3.38	4.25	-0.20 ± 0.42
BPBE	2.55	4.54	2.56	4.80	3.34	3.41	4.29	0.03 ± 0.24
M06	2.13	3.69	2.60	4.48	3.53	3.42	4.38	-0.11 ± 0.38
M062X	1.39	2.89	2.36	4.58	3.50	3.38	4.41	-0.28 ± 0.63
BLYP	2.67	4.69	2.87	4.55	3.45	3.50	4.47	0.13 ± 0.31
TPSS	2.69	4.52	2.92	4.61	3.51	3.57	4.62	0.16 ± 0.30
PBE	2.89	4.86	2.73	4.94	3.37	3.46	4.27	0.14 ± 0.34

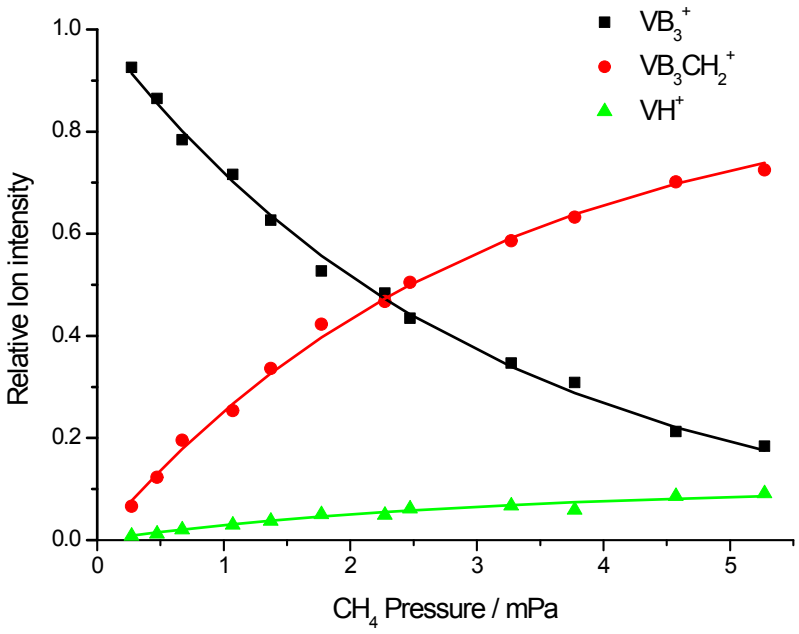

Figure S1. Variations of relative ion intensities with respect to the CH_4 pressure in the reaction of VB_3^+ with CH_4.

The relative intensities of the reactant ions (I_R, VB_3^+) and product ions (I_P, $VB_3CH_2^+$ and VH^+) can be fitted by using the following equations:

$$\ln\frac{I_R}{I_R+I_P} = -k_1\frac{P}{k_BT}t_R$$

where k_1 is the pseudo first-order rate constant, P is the pressure of the reactant molecules (CH_4), k_B is the Boltzmann constant, T is the temperature (~300 K), and t_R is the interaction time (~ 1.9 ms).

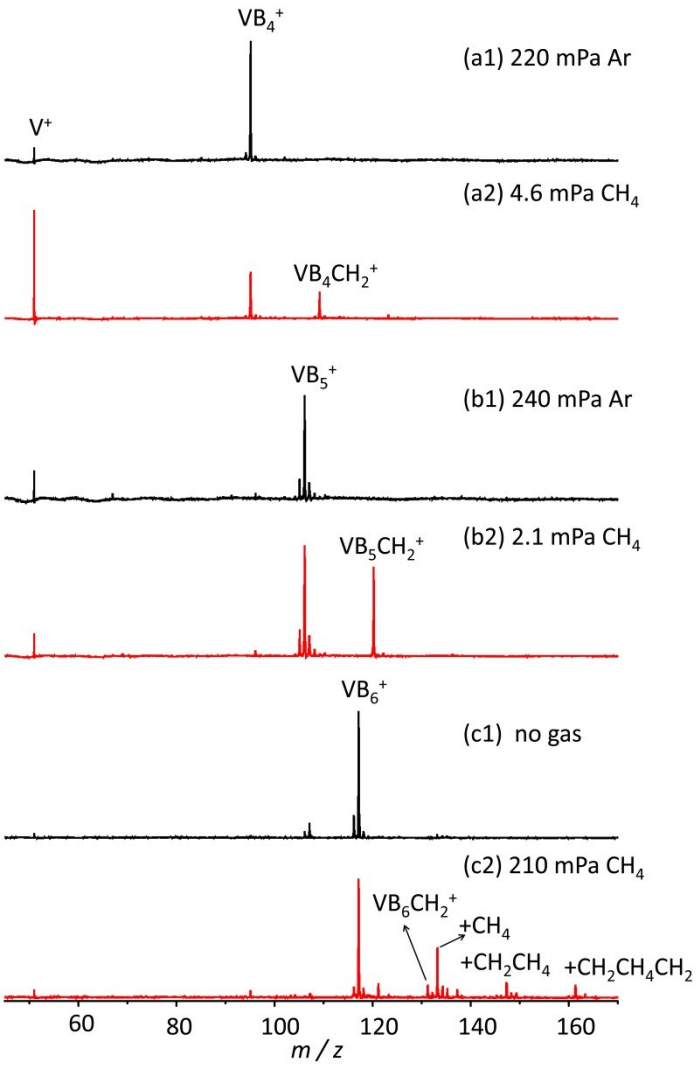

Figure S2. The time-of-flight (TOF) mass spectra for reactions of mass-selected VB_n^+ (n = 4–6) with Ar (a1 and b1) and CH_4 (a2, b2 and c2) in an ion trap reactor for about 1.9 ms. The peaks marked with +X (X = CH_4, CH_2CH_4, and $CH_2CH_4CH_2$) in c2 denote VB_6X^+. The reactant gas pressures are given.

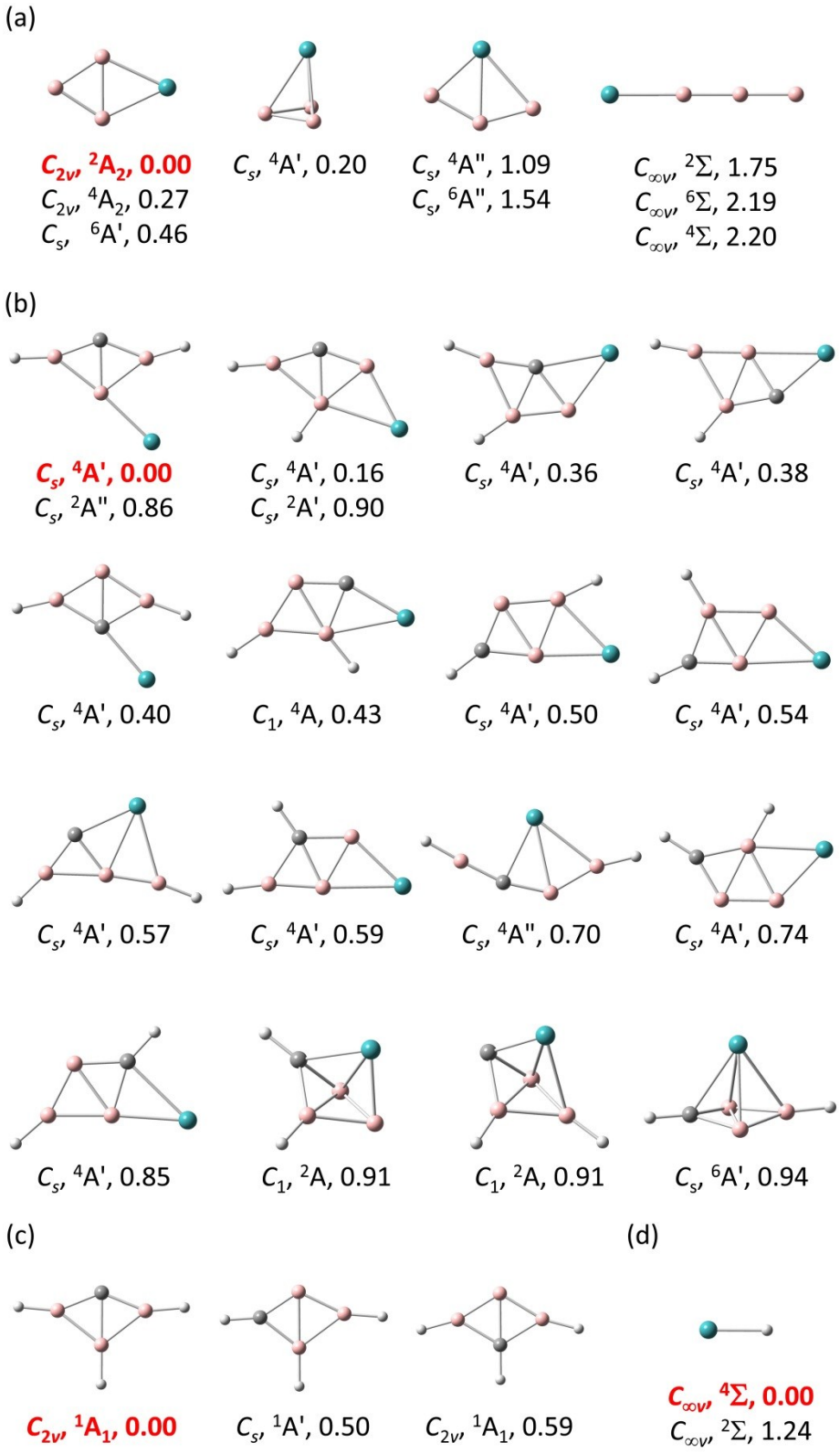

Figure S3. Low-lying isomers of (a) VB_3^+, (b) $VB_3CH_2^+$, (c) B_3CH_3 and (d) VH^+ at M06L/TZVP level. The symmetry, electronic state, and the zero-point vibration corrected energies (ΔH_0, in eV) with respect to the most stable isomer are given. The superscript denotes spin multiplicity.

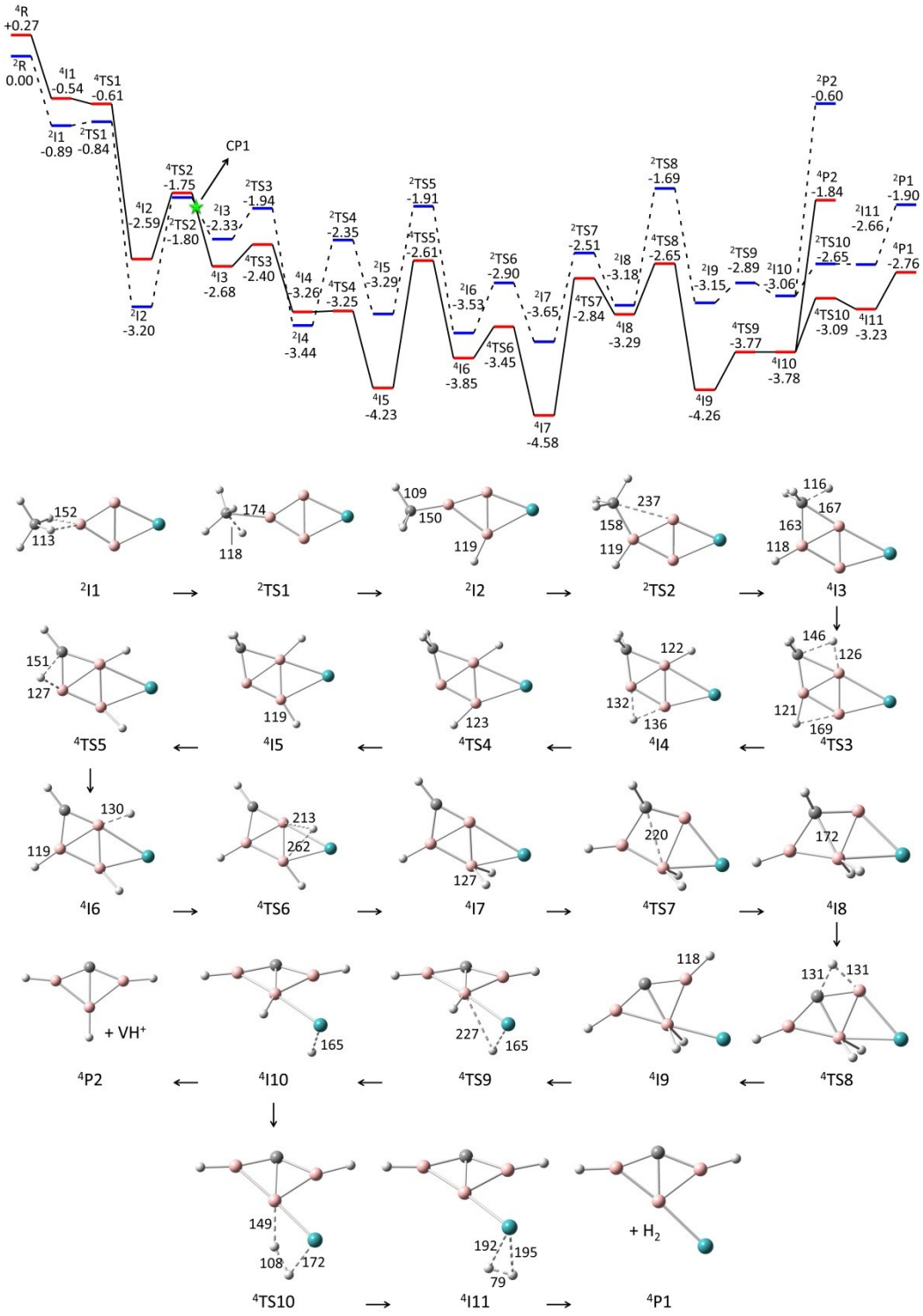

Figure S4. DFT calculated potential energy profiles for the reaction of VB_3^+ with CH_4 starting from the B_3 moiety. The superscript denotes spin multiplicity. The structures of the intermediates (^{2}I1−^{2}I2 and ^{4}I3−^{4}I11), transition states (^{2}TS1−^{2}TS2 and ^{4}TS3−^{4}TS10), and products (^{4}P1 and ^{4}P2) are shown. The crossing point (CP1) appearing in the spin conversion is shown in Figure S6. The zero-point vibration corrected energies (ΔH_0) with respect to the separated reactants and the bond lengths are given in eV and pm, respectively.

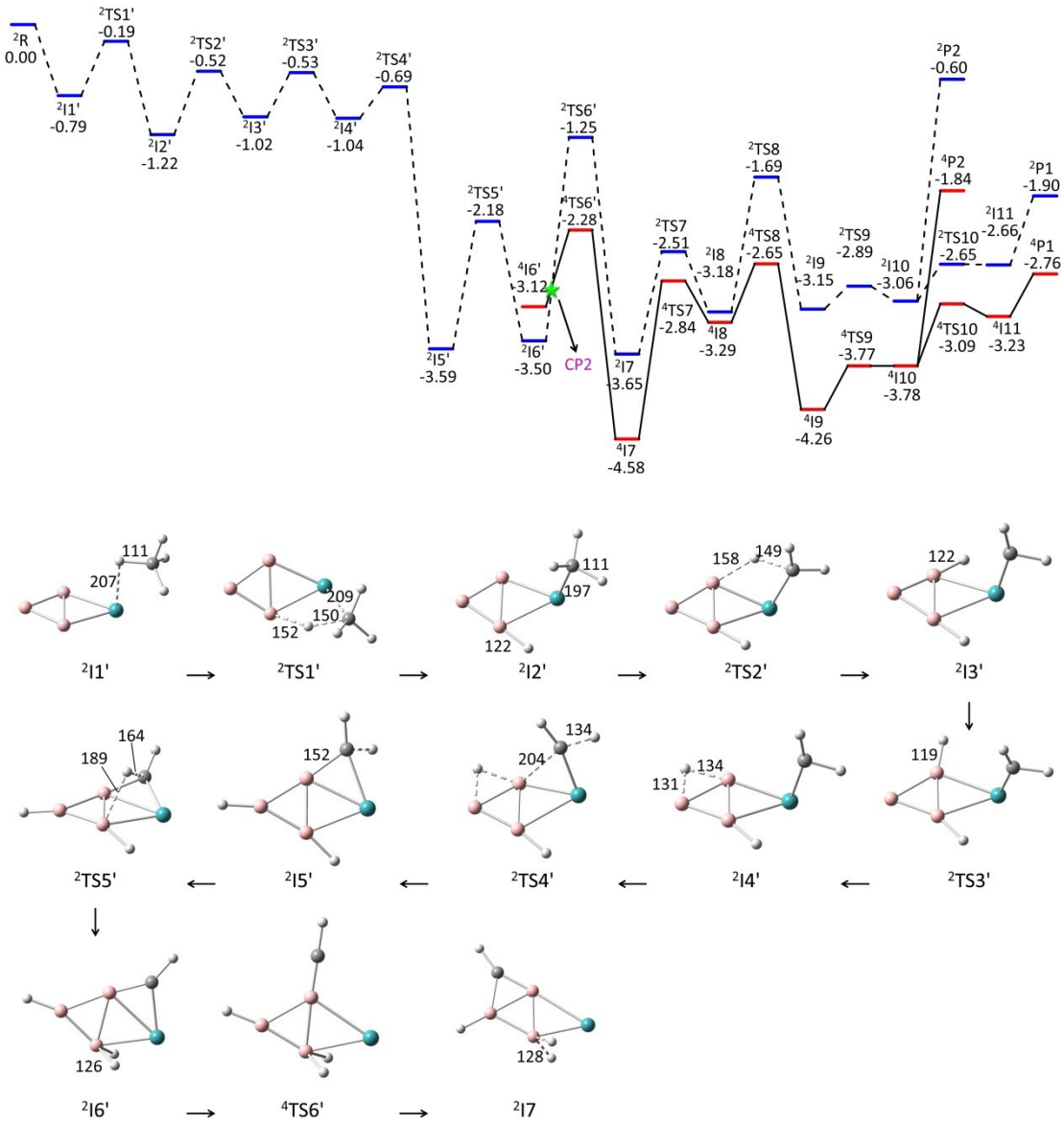

Figure S5. DFT calculated potential energy profiles for the reaction of VB_3^+ with CH_4 starting from the V side. The superscript denotes spin multiplicity. The structures of the intermediates (^{2}I1'–^{2}I6') and transition states (^{2}TS1'–^{2}TS5' and ^{4}TS6') are shown. The structures of intermediates (^{4}I8–^{4}I11), transition states (^{4}TS7–^{4}TS10), and products (^{4}P1 and ^{4}P2) can be found in Figure S5. The crossing point (CP2) appearing in the spin conversion is shown in Figure S6. The zero-point vibration corrected energies (ΔH_0) with respect to the separated reactants and the bond lengths are given in eV and pm, respectively.

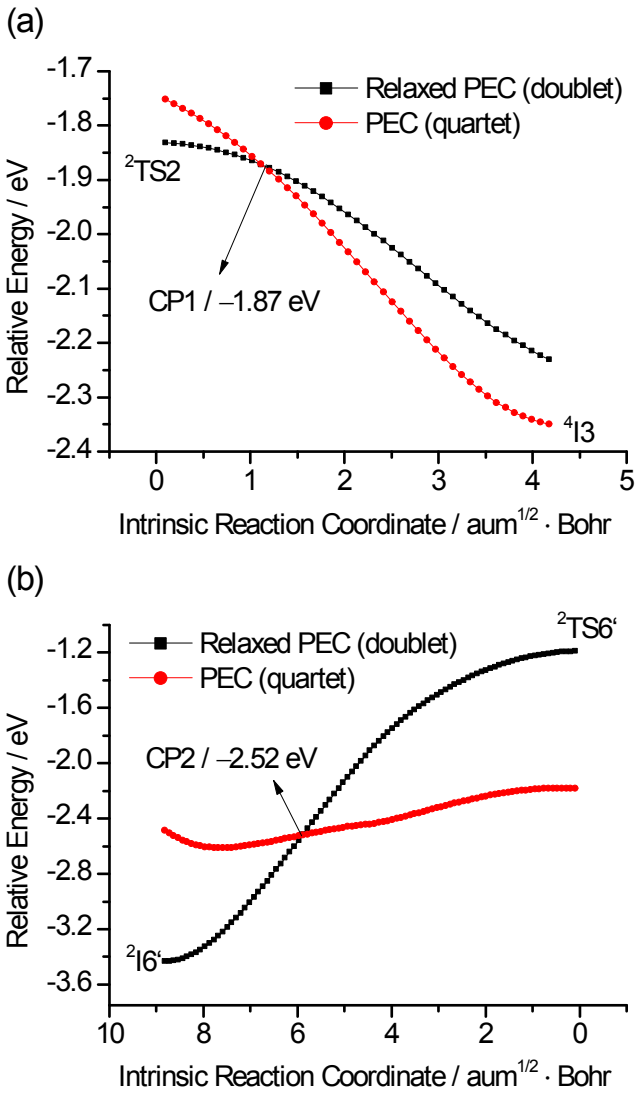

Figure S6. DFT-calculated potential-energy curves (PECs) for spin conversions in Figures S4 and S5. The filled square lines in (a-b) are the relaxed PECs obtained by IRC calculations starting from ^{2}TS2 to ^{2}I3 and ^{2}TS6' to ^{2}I6', respectively. The optimized geometries from the filled square line (doublet) in (a-b) were used for single-point energy calculations of the quartet (filled circle line), respectively. The energies of the crossing points (CP1 and CP2) relative to the separated reactants ($^2VB_3^+ + CH_4$) are given.

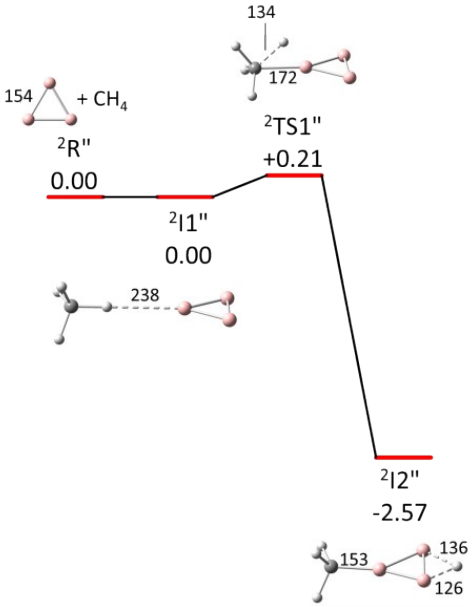

Figure S7. DFT calculated potential energy profile for the reaction of neutral B_3 cluster with CH_4. The superscript denotes spin multiplicity. The zero-point vibration corrected energies (ΔH_0) with respect to the separated reactants and the bond lengths are given in eV and pm, respectively.

References

S1 a) X.-N. Wu, J.-B. Ma, B. Xu, Y.-X. Zhao, X.-L. Ding and S.-G. He, *J. Phys. Chem. A* 2011, **115**, 5238-5246. b) X.-N. Wu, B. Xu, J.-H. Meng and S.-G. He, *Int. J. Mass Spectrom.*, 2012, **310**, 57-64.

S2 Z. Yuan, Y.-X. Zhao, X.-N. Li and S.-G. He, *Int. J. Mass Spectrom.*, 2013, **354-355**, 105-112.

S3 Z. Yuan, Z.-Y. Li, Z.-X. Zhou, Q.-Y. Liu, Y.-X. Zhao and S.-G. He, *J. Phys. Chem. C*, 2014, **118**, 14967-14976.

S4 M. J. Frisch, G. W. Trucks, H. B. Schlegel, G. E. Scuseria, M. A. Robb, J. R. Cheeseman, G. Scalmani, V. Barone, B. Mennucci, G. A. Petersson, H. Nakatsuji, M. Caricato, X. Li, H. P. Hratchian, A. F. Izmaylov, J. Bloino, G. Zheng, J. L. Sonnenberg, M. Hada, M. Ehara, K. Toyota, R. Fukuda, J. Hasegawa, M. Ishida, T. Nakajima, Y. Honda, O. Kitao, H. Nakai, T. Vreven, J. A. Montgomery, Jr., J. E. Peralta, F. Ogliaro, M. Bearpark, J. J. Heyd, E. Brothers, K. N. Kudin, V. N. Staroverov, R. Kobayashi, J. Normand, K. Raghavachari, A. Rendell, J. C. Burant, S. S. Iyengar, J. Tomasi, M. Cossi, N. Rega, J. M. Millam, M. Klene, J. E. Knox, J. B. Cross, V. Bakken, C. Adamo, J. Jaramillo, R. Gomperts, R. E. Stratmann, O. Yazyev, A. J. Austin, R. Cammi, C. Pomelli, J. W. Ochterski, R. L. Martin, K. Morokuma, V. G. Zakrzewski, G. A. Voth, P. Salvador, J. J. Dannenberg, S. Dapprich, A. D. Daniels, O. Farkas, J. B. Foresman, J. V. Ortiz, J. Cioslowski and D. J. Fox, Gaussian 09, Revision A.1; Gaussian, Inc., Wallingford, CT, 2009.

S5 A. Schäfer, C. Huber and R. Ahlrichs, *J. Chem. Phys.*, 1994, **100**, 5829-5835.

S6 J. Alistair Kerr, Strengths of Chemical Bonds. In *Handbook of Chemistry and Physics, 84th ed.*; D. R. Lide, Ed; CRC: Boca Raton, 2003; Sect. 9, pp. 52-64.

S7 Y. Zhao and D. G. Truhlar, *J. Chem. Phys.*, 2006, **125**, 194101.

S8 J.-B. Ma, B. Xu, J.-H. Meng, X.-N. Wu, X.-L. Ding, X.-N. Li and S.-G. He, *J. Am. Chem. Soc.* 2013, **135**, 2991-2998.

S9 I. Berente and G. Naray-Szabo, *The journal of physical chemistry. A*, 2006, **110**, 772-778.

S10 H. B. Schlegel, *J. Comput. Chem.*, 1982, **3**, 214-218.

S11 C. Gonzalez and H. B. Schlegel, *J. Chem. Phys.*, 1989, **90**, 2154-2161.

S12 E. D. Glendening, A. E. Reed, J. E. Carpenter and F. Weinhold, *NBO 3.1*, Theoretical Chemistry Institute, University of Wisconsin, Madison, WI, 1996.